CO Multi-line Imaging of Nearby Galaxies (COMING). X. Physical conditions of molecular gas and the local SFR–mass relation

Kana MOROKUMA-MATSUI [1,2,*,†] Kazuo SORAI [3,4,5,6] Yuya SATO,[5] Nario KUNO [5,6] Tsutomu T. TAKEUCHI [7,8] Dragan SALAK [6] Yusuke MIYAMOTO [2] Yoshiyuki YAJIMA [4] Kazuyuki MURAOKA [9] and Hiroyuki KANEKO [2,10]

[1]Institute of Astronomy, Graduate School of Science, The University of Tokyo, 2-21-1 Osawa, Mitaka, Tokyo 181-0015, Japan

[2]National Astronomical Observatory of Japan, National Institutes of Natural Sciences, 2-21-1 Osawa, Mitaka, Tokyo 181-8588, Japan

[3]Department of Physics, Faculty of Science, Hokkaido University, Kita 10 Nishi 8, Kita-ku, Sapporo, Hokkaido 060-0810, Japan

[4]Department of Cosmosciences, Graduate School of Science, Hokkaido University, Kita 10 Nishi 8, Kita-ku, Sapporo, Hokkaido 060-0810, Japan

[5]Department of Physics, Graduate School of Pure and Applied Sciences, University of Tsukuba, 1-1-1 Tennodai, Tsukuba, Ibaraki 305-8577, Japan

[6]Tomonaga Center for the History of the Universe, University of Tsukuba, 1-1-1 Tennodai, Tsukuba, Ibaraki 305-8571, Japan

[7]Division of Particle and Astrophysical Science, Nagoya University, Furo-cho, Chikusa-ku, Nagoya, Aichi 464-8602, Japan

[8]The Research Center for Statistical Machine Learning, the Institute of Statistical Mathematics, 10-3 Midori-cho, Tachikawa, Tokyo 190-8562, Japan

[9]Department of Physical Science, Graduate School of Science, Osaka Prefecture University, 1-1 Gakuen-cho, Naka-ku, Sakai, Osaka 599-8531, Japan

[10]Graduate School of Education, Joetsu University of Education, 1 Yamayashiki-machi, Joetsu, Niigata 943-8512, Japan

*E-mail: kanamoro@ioa.s.u-tokyo.ac.jp

†JSPS Fellow

Abstract

We investigate the molecular gas properties of galaxies across the main sequence of star-forming (SF) galaxies in the local Universe using $^{12}CO(J = 1–0)$, hereafter ^{12}CO, and $^{13}CO(J = 1–0)$, hereafter ^{13}CO, mapping data of 147 nearby galaxies obtained in the COMING project, a legacy project of the Nobeyama Radio Observatory. In order to improve the signal-to-noise ratios of both lines, we stack all the pixels where ^{12}CO emission is detected after aligning the line center expected from the first-moment map of ^{12}CO. As a result, ^{13}CO emission is successfully detected in 80 galaxies with a signal-to-noise ratio larger than three. The error-weighted mean of the integrated-intensity ratio

of ^{12}CO to ^{13}CO lines (R_{1213}) of the 80 galaxies is 10.9, with a standard deviation of 7.0. We find that (1) R_{1213} positively correlates to specific star-formation rate (sSFR) with a correlation coefficient of 0.46, and (2) both the flux ratio of IRAS 60 μm to 100 μm (f_{60}/f_{100}) and the inclination-corrected linewidth of ^{12}CO stacked spectra ($\sigma_{^{12}CO,i}$) also correlate with sSFR for galaxies with the R_{1213} measurement. Our results support the scenario where R_{1213} variation is mainly caused by changes in molecular gas properties such as temperature and turbulence. The consequent variation of the CO-to-H$_2$ conversion factor across the SF main sequence is not large enough to completely extinguish the known correlations between sSFR and M_{mol}/M_{star} (μ_{mol}) or star-formation efficiency (SFE) reported in previous studies, while this variation would strengthen (weaken) the sSFR–SFE (sSFR–μ_{mol}) correlation.

Key words: galaxies: evolution — galaxies: ISM — galaxies: kinematics and dynamics — radio lines: galaxies

1 Introduction

Galaxies show distinctive distributions on the plot of stellar mass (M_{star}) against star-formation rate (SFR): some galaxies are on the sequence showing a positive correlation between the two values, and some locate far below the correlation in the SFR direction. The former are called the main sequence of star-forming (SF) galaxies (hereafter SF main sequence, e.g., Noeske et al. 2007; Elbaz et al. 2007; Daddi et al. 2007) and the latter are called quenched or passive galaxies. Investigating how the galaxy properties change along and across the SF main sequence leads to essential understanding of galaxy evolution (e.g., Wuyts et al. 2011). Provided that stars are formed in molecular clouds in the local Universe, it is vital to study the molecular gas properties along and across the SF main sequence.

It has been reported that there are positive correlations between specific SFR [sSFR = SFR/M_{star}, or an offset from the SF main sequence, Δ(MS)] with the molecular gas mass (M_{mol}) to M_{star} ratio ($\mu_{mol} = M_{mol}/M_{star}$) and star-formation efficiency (SFE = SFR/M_{mol}), i.e., galaxies with higher sSFR tend to have more abundant molecular gas and form stars more efficiently from the molecular gas (e.g., Saintonge et al. 2012; Genzel et al. 2015; Scoville et al. 2017; Tacconi et al. 2018). These correlations still hold for spatially resolved data (Lin et al. 2017; Ellison et al. 2020a, 2020b; M. Kajikawa in preparation). In addition, it is known that these correlations are irrespective of the environment (Koyama et al. 2017) or the mass concentration of stellar components of galaxies (Koyama et al. 2019), indicating their importance for galaxy evolution. Furthermore, recent studies have claimed that the scatter of the SF main sequence is primarily due to the SFE variety with a secondary role for μ_{mol}, using spatially resolved molecular gas data and optical integral field unit data (Ellison et al. 2020a).

Molecular rotational transitions have been used to explore the physical properties of molecular gas in galaxies. Especially, the lowest transition lines ($J = 1$–0) of carbon monoxide, ^{12}CO, and its isotopes are ideal tracers of cold ($\sim$10 K) molecular gas which is the raw material of star formation, since the corresponding energy gaps ($h\nu_{rest}$, where h is the Planck constant and ν_{rest} is the rest frequency of the line) divided by the Boltzmann constant are $\sim$5.53 K for ^{12}CO($J = 1$–0)—$\nu_{rest} = 115.271$ GHz, hereafter ^{12}CO— and $\sim$5.29 K for ^{13}CO($J = 1$–0)—$\nu_{rest} = 110.201$ GHz, hereafter ^{13}CO—respectively. ^{12}CO emission is generally optically thick but strong even in extragalactic objects, thus it is widely used to measure the molecular gas mass of galaxies by assuming CO-to-H$_2$ conversion factors (e.g., Rickard et al. 1975; Solomon & de Zafra 1975; Young & Scoville 1982; Bolatto et al. 2013, and references therein). On the other hand, ^{13}CO is used as an optically thin tracer of molecular gas and is known to be well correlated with dust extinction in molecular clouds in the Milky Way (e.g., Dickman 1978; Frerking et al. 1982; Lada et al. 1994).

Detailed studies of the line ratio of ^{12}CO/^{13}CO (hereafter R_{1213}) have revealed a wide variety of R_{1213} within the Milky Way. In a giant molecular cloud (GMC) where stars are formed, R_{1213} is reported to be $\sim$3 at the center and $\sim$5 for the whole cloud (Gordon & Burton 1976; Solomon et al. 1979; Polk et al. 1988), which are much smaller than the abundance ratio of [^{12}CO]/[^{13}CO] inferred from the ^{12}C/^{13}C ratio, which has a radial gradient, with $\sim$20 at the galaxy center and $\sim$60 in the Solar neighborhood (Milam et al. 2005; Halfen et al. 2017). This suggests that the bulk of ^{12}CO emission is optically thick in GMCs. On the other hand, larger R_{1213} values are reported in the peripheries of GMCs ($R_{1213} \sim 20$, Sakamoto et al. 1994), high-latitude molecular clouds ($\sim$10.5, Blitz et al. 1984), and small molecular clouds with a size of $<$1.0 pc ($\sim$40, Knapp & Bowers 1988), suggesting a lower optical depth of ^{12}CO line in those components than in GMCs. Polk et al. (1988) obtained a relatively high R_{1213} value of $\sim$7 when they calculated the average R_{1213} value of seven

$0°5 \times 0°5$ regions in the Galactic plane and suggested a non-negligible contribution of the lower-optical-depth (diffuse) molecular gas to the large-scale ^{12}CO emission of the Milky Way.

Since the early studies of CO isotopes of local galaxies in the 1970s (Encrenaz et al. 1979; upper limits by Rickard et al. 1977), various and reasonably larger R_{1213} values than those of GMCs have been reported in nearby galaxies, for example a typical R_{1213} of ~ 10 in spiral galaxies (e.g., Young & Scoville 1982; Young & Sanders 1986; Weliachew et al. 1988; Sandqvist et al. 1988; Sage & Isbell 1991; Wright et al. 1993; Braine et al. 1993; Aalto et al. 1994; Xie et al. 1994; Matsushita et al. 1998; Paglione et al. 2001; Hirota et al. 2010; Watanabe et al. 2011; Davis 2014; Vila-Vilaro et al. 2015; Morokuma-Matsui et al. 2015; Cormier et al. 2018; Lee & Chung 2018), ~ 10 in early-type galaxies (ETGs, e.g., Eckart et al. 1990; Sage 1990; Wild et al. 1997; Crocker et al. 2012; Davis 2014; Alatalo et al. 2015), ~ 15 in irregular galaxies (e.g., Becker & Freudling 1991), ~ 30 in merging galaxies (e.g., Aalto et al. 1991, 1997, 2010; Casoli et al. 1992; Taniguchi & Ohyama 1998), starburst galaxies (e.g., Stark & Carlson 1984; Young & Scoville 1984; Kikumoto et al. 1998), and infrared-bright galaxies (e.g., Garay et al. 1993; Aalto et al. 1995; Cao et al. 2017; Sliwa et al. 2017; Herrero-Illana et al. 2019), ~ 10 in Seyfert galaxies (e.g., Papadopoulos & Seaquist 1998, 1999), and ~ 30 in $z \sim 3$ galaxies with $J > 1$ transitions (e.g., Henkel et al. 2010; Danielson et al. 2013; Spilker et al. 2014; Béthermin et al. 2018). The large R_{1213} values could reflect the presence of a substantial amount of low-optical-depth (diffuse) components in those galaxies (e.g., Polk et al. 1988; Garcia-Burillo et al. 1992; Aalto et al. 1995; Sakamoto et al. 1997; Hirota et al. 2010; Morokuma-Matsui et al. 2015). These studies are suggestive of a dependence of R_{1213} on SF activities in galaxies, but the relationship between R_{1213} and sSFR or Δ(MS) has not been systematically explored so far.

In this study we compare the R_{1213} and sSFR of galaxies targeted in the CO Multi-line Imaging of Nearby Galaxies project (COMING, Sorai et al. 2019), a legacy project making use of the 45 m radio telescope at the Nobeyama Radio Observatory[1] in order to investigate the molecular gas properties across the SF main sequence of galaxies. The COMING project *simultaneously* obtained ^{12}CO, ^{13}CO, and $C^{18}O(J = 1–0)$ mapping data of 147 galaxies with various sSFR located at distances of $\lesssim 40$ Mpc, which makes it one of the largest mapping surveys of galaxies in multiple CO isotopes. Provided that the ^{12}CO and ^{13}CO data in

the COMING project are obtained in the same observing conditions, including the accuracy of the telescope pointings, R_{1213} measurements do not suffer from the relevant uncertainties.

The structure of this paper is as follows. We first briefly describe the data we used and the data analysis, specifically stacking analysis, in section 2, and we present the basic properties and the relationship between R_{1213} and sSFR of our sample galaxies in section 3. Based on the results, we discuss the origin of the R_{1213} variation and its implication for the consequent variety in the CO-to-H_2 conversion factor (α_{CO}) in local galaxies as well as high-redshift galaxies in section 4, and then we summarize this study in section 5. Throughout, we assume the Kroupa initial mass function (IMF, Kroupa 2001; Kroupa & Weidner 2003). For a correlation check, we refer to three values: Pearson's correlation coefficient r, Spearman's rank correlation coefficient ρ, and Kendall's rank correlation coefficient τ. The first one is a parametric measure and the latter two are non-parametric measures. Although the obtained values are different from method to method, the overall trends are almost consistent across the three methods. We basically adopt the widely used Spearman's ρ to discuss the correlation of the two galaxy parameters in this paper.

2 Data and analysis

In this study we used the physical parameters of the COMING galaxies such as M_{star}, SFR, sSFR, M_{mol}, SFE, μ_{mol}, R_{1213}, and the velocity dispersion of stacked ^{12}CO spectra. We briefly discuss the derivation of these parameters from the observed data in this section.

2.1 Molecular lines: COMING ^{12}CO and ^{13}CO data

We used ^{12}CO and ^{13}CO data obtained in the COMING project (Sorai et al. 2019) to calculate the integrated intensity ratio,

$$R_{1213} = I_{^{12}CO}/I_{^{13}CO}, \tag{1}$$

where $I_{^{12}CO}$ and $I_{^{13}CO}$ are the integrated intensities in units of $K\,km\,s^{-1}$ of the ^{12}CO and ^{13}CO emission lines, respectively. The angular and velocity resolutions of the COMING data are $\sim 17''$ (~ 1.6 kpc at 20 Mpc) and $10\,km\,s^{-1}$, respectively. We stacked all the ^{12}CO and ^{13}CO spectra of pixels where ^{12}CO emission is detected with a signal-to-noise ratio of larger than three for each galaxy after aligning the line center expected from the first-moment map of the ^{12}CO line (hereafter, "VA" stacking; Schruba et al. 2011; Caldú-Primo et al. 2013; Morokuma-Matsui et al. 2015). The number of stacked pixels differs from

---

[1] The Nobeyama 45 m radio telescope is operated by Nobeyama Radio Observatory, a branch of the National Astronomical Observatory of Japan.

galaxy to galaxy and ranges from 20 to 2431 (the median, first, and third quartiles are 274.5, 154.5, and 447.5, respectively).[2] With the VA stacking analysis, the ^{13}CO emission line was detected in 80 galaxies with a signal-to-noise ratio of >3. It should be noted that the number of galaxies with a "secure" detection of ^{13}CO emission in the original data (more than three pixels with $\geq 4\sigma$ detection in the ^{13}CO integrated intensity and $\geq 3\sigma$ detection in the ^{12}CO integrated intensity) is only 52 (Sorai et al. 2019).

The velocity dispersions of stacked ^{12}CO spectra, $\sigma_{^{12}\mathrm{CO}}$, are derived by single Gaussian fitting. Since this value encompasses both random motion among clouds and/or volume-filling gas and the velocity gradient due to galactic rotation within the ~ 1 kpc beam, we correct for the effect of inclination (i) by dividing the value by $\sin(i)$, $\sigma_{^{12}\mathrm{CO},i} = \sigma_{^{12}\mathrm{CO}}/\sin(i)$. ^{12}CO data is also used to calculate the molecular gas mass of galaxies. We adopt M_{mol} from Sorai et al. (2019), which assumed the standard CO-to-H$_2$ conversion factor of the Milky Way of 2.0×10^{20} cm^{-2} (K km s^{-1})$^{-1}$ (Bolatto et al. 2013).

2.2 Stellar mass and SFR: WISE and GALEX

We adopt M_{star} values derived by Sorai et al. (2019), who used $3.4\,\mu$m data obtained with the Wide-field Infrared Survey Explorer (WISE, Wright et al. 2010) and an empirical relation between $3.4\,\mu$m luminosity and M_{star} presented by Wen et al. (2013) assuming the Kroupa IMF. Sorai et al. (2019) reported that their M_{star} values were $\sim 20\%$ lower than those calculated in the Spitzer Survey of Stellar Structure in Galaxies project (S^{4}G, Sheth et al. 2010) due to their conservative subtraction of foreground stars. The SFR map of the COMING galaxies is generated using WISE $22\,\mu$m and far-ultraviolet (FUV) imaging data obtained with the Galaxy Evolution Explorer (GALEX, Martin et al. 2005) as

$$\Sigma_{\mathrm{SFR}} = 3.2 \times 10^{-3} \times I_{22\mu m} + 8.1 \times 10^{-2} \times I_{\mathrm{FUV}}, \quad (2)$$

where Σ_{SFR} is SFR surface densities in units of $M_{\odot}$ yr^{-1} kpc^{-2}, and $I_{22\mu m}$ and I_{FUV} are te WISE/22 μm and GALEX/FUV intensities, respectively, in units of MJy sr^{-1} (Casasola et al. 2017). The SFR calibration method adopted by Casasola et al. (2017) assumes the default IMF in STATBURST99 (Leitherer et al. 1999). To convert from the SFR with the STATBURST99 IMF to the SFR with the Salpeter IMF (Salpeter 1955), one should multiply the value by 1.59. Furthermore, to convert from the SFR with the

Salpeter IMF to the SFR with the Kroupa IMF, one should multiply the value by 0.67. The details of estimating SFR and star-formation properties will be presented in a forthcoming paper (T. T. Takeuchi et al. in preparation). In this study we limit our sample to the COMING galaxies with both the WISE $22\,\mu$m and the GALEX FUV detections, resulting in 107 galaxies. The number of galaxies with M_{star} and SFR measurements and ^{13}CO detections reduces to 63. The 63 galaxies consist of spiral galaxies (S, SA, SAB, or SB classifications in the Third Reference Catalogue of Bright Galaxies, RC3; de Vaucouleurs et al. 1991) and no interacting galaxies, irregular galaxies, or ETGs are included.

2.3 Dust emission: IRAS 60 μm and 100 μm data

We crossmatch the 147 COMING galaxies with the IRAS Revised Bright Galaxy Sample (RBGS, Sanders et al. 2003), which lists total fluxes covering extended emission of galaxies in the IRAS bands. The IRAS RBGS consists of 629 galaxies with 60 μm flux of >5.24 Jy. The matching results in 111 galaxies, and 62 have all the measurements of M_{star}, SFR, stacked ^{12}CO and ^{13}CO emissions, and IRAS fluxes at 60 μm and 100 μm.

3 Results

In figure 1 we present the basic properties of the COMING galaxies and compare them with galaxies in the extended CO Legacy Database for the GASS project (xCOLD GASS, Saintonge et al. 2011, 2017), which is the largest ^{12}CO survey, targeting 532 galaxies at $0.01 < z < 0.05$. The SF main sequence in the local Universe (Speagle et al. 2014) is also indicated by the solid cyan line as a reference in panel (a). We can see that most of the COMING sample is above or on the SF main sequence, and some are located in the so-called "green valley" regime. It should be noted that our sSFR estimations of the COMING galaxies are expected to be higher than those in the literature since the adopted M_{star} values are known to be $\sim 20\%$ lower than the previous studies, as mentioned in subsection 2.2. Overall, the COMING and the CO-detected xCOLD GASS galaxies share similar star-formation properties such as sSFR, SFE, and μ_{mol}. Panel (c) of the same figure shows that galaxies without ^{13}CO detection, indicated as open black circles, tend to have low μ_{mol} and/or high sSFR values.

The error-weighted mean and standard deviation of R_{1213} for the 80 COMING galaxies with ^{12}CO and ^{13}CO measurements are 10.9 and 7.0, respectively. If we limit the sample to the 63 galaxies that are plotted in figure 2a, these values become 11.4 (mean) and 6.7 (standard deviation). This is consistent with previous studies on R_{1213} of local star-forming galaxies (~ 10–15, e.g., Young & Sanders

---

[2] Since the number of galaxies with ^{13}CO detection is even (80), the median, first, and third quartiles are calculated as the means of the central two values of the whole sample, the first quarter sample, and the last quarter sample, respectively, when the galaxies are sorted according to the number of stacked pixels.
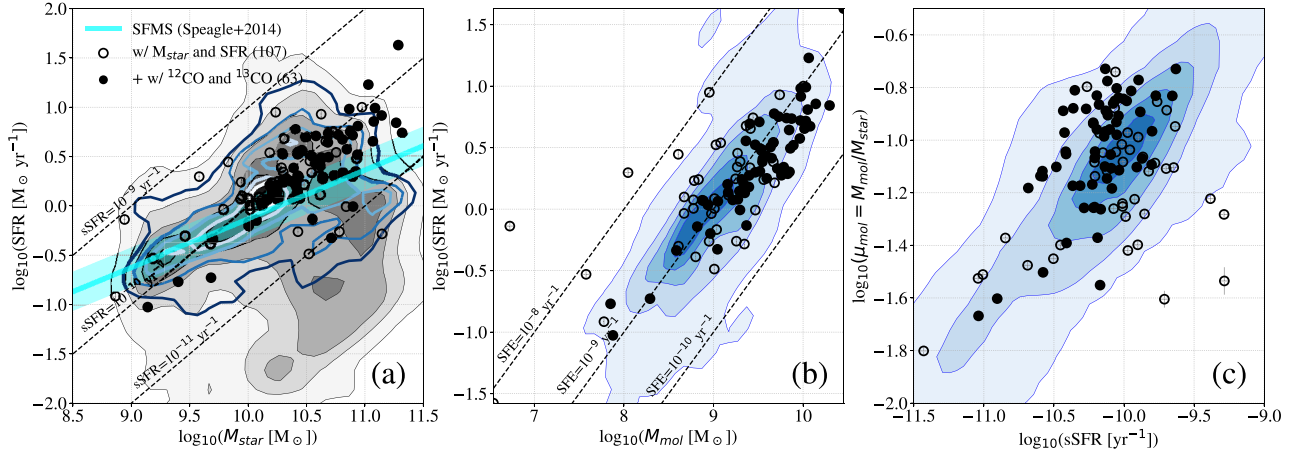
Fig. 1. Basic properties of the COMING galaxies: (a) the M_{star}–SFR relation, (b) the M_{mol}–SFR ("Kennicutt–Schmidt") relation, and (c) the sSFR–μ_{mol} relation. COMING galaxies are indicated as circle symbols, and among them, those with R_{1213} measurements are indicated as filled black circles. In panel (a), the gray-filled contour indicates galaxies observed in the xCOLD GASS project, and the thick contours with different shades of blue indicate xCOLD GASS galaxies with CO detection (Saintonge et al. 2011, 2017). The SF main sequence at $z = 0$ is indicated as a solid cyan line, and the 0.2 dex scatter range is indicated as cyan shading (Speagle et al. 2014). In panels (b) and (c), the blue-filled contour indicates xCOLD GASS galaxies with CO detection, which are the same galaxies as those indicated by thick contours in panel (a). (Color online)
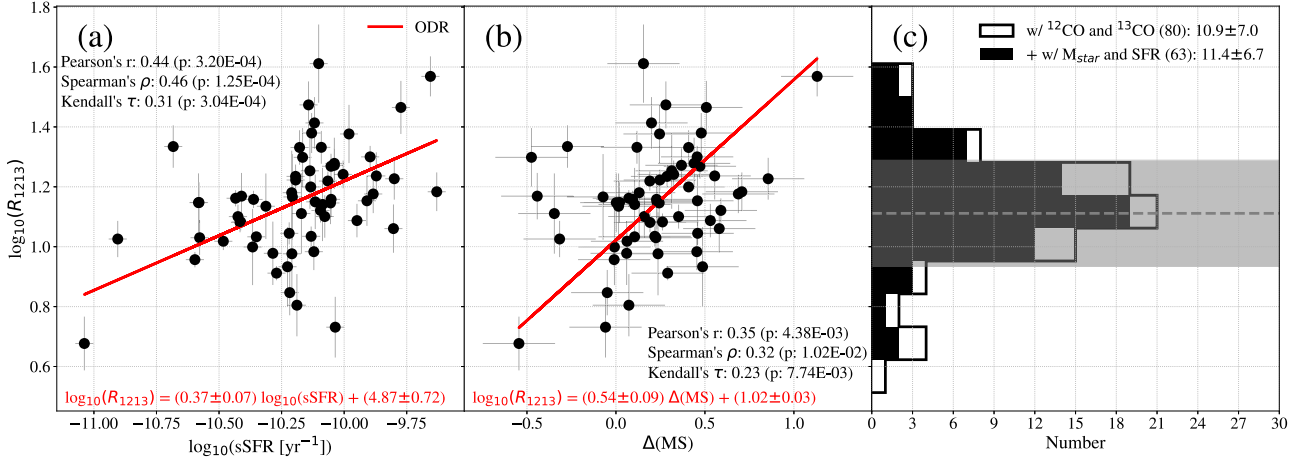

Fig. 2. Obtained relations between (a) R_{1213} and sSFR and (b) R_{1213} and Δ(MS) of the 63 COMING galaxies. Panel (c) shows a histogram of the R_{1213} values for the 80 galaxies with R_{1213} measurements and the 63 galaxies with both R_{1213} and sSFR measurements. The fitting functions with ODR are presented at the bottom of panels (a) and (b). The gray dashed line and gray shaded regions in panel (c) indicate the error-weighted mean and standard deviation of the 63 COMING galaxies. (Color online)

1986; Paglione et al. 2001; Vila-Vilaro et al. 2015). Using the R_{1213} and sSFR of the 63 galaxies, we find a moderate correlation between these two values with a Spearman rank correlation coefficient ρ of 0.46 (see figure 2a). The possibility of a fake correlation for the R_{1213}–sSFR relation is discussed in the Appendix. The fitting function by orthogonal distance regression (ODR) is shown in this figure.

We also examine the relationship between R_{1213} and the SFR offset from the SF main sequence, Δ(MS), which is calculated as

$$\Delta(\text{MS}) = \log(\text{SFR}) - \log[\text{SFR}_{\text{MS}}(M_{\text{star}}, t)], \quad (3)$$

where $\text{SFR}_{\text{MS}}(M_{\text{star}}, t)$ is the SFR of the SF main-sequence galaxies with a mass of M_{star} [$M_{\odot}$] at the age of the Universe

of t [Gyr], which is calculated as

$$\log[\text{SFR}_{\text{MS}}(M_{\text{star}}, t)] = (0.84 - 0.026)\log(M_{\text{star}})$$
$$- (6.51 - 0.11t) \quad (4)$$

(Speagle et al. 2014).[3] Here we adopt the same cosmology parameters as Speagle et al. (2014), $(h, \Omega_M, \Omega_\Lambda) = (0.7, 0.3, 0.7)$, to calculate the age of the Universe at $z = 0$. Compared to sSFR, R_{1213} seems to similarly but rather weakly correlate with Δ(MS). It should be noted that this tendency does not change even if another widely used definition of the SF

---

[3] Speagle et al. (2014) compiled 64 observations of main-sequence galaxies at $0 < z < 6$ from 25 studies and derived the SF main sequence as a function of redshift after converting them to the same calibrations.
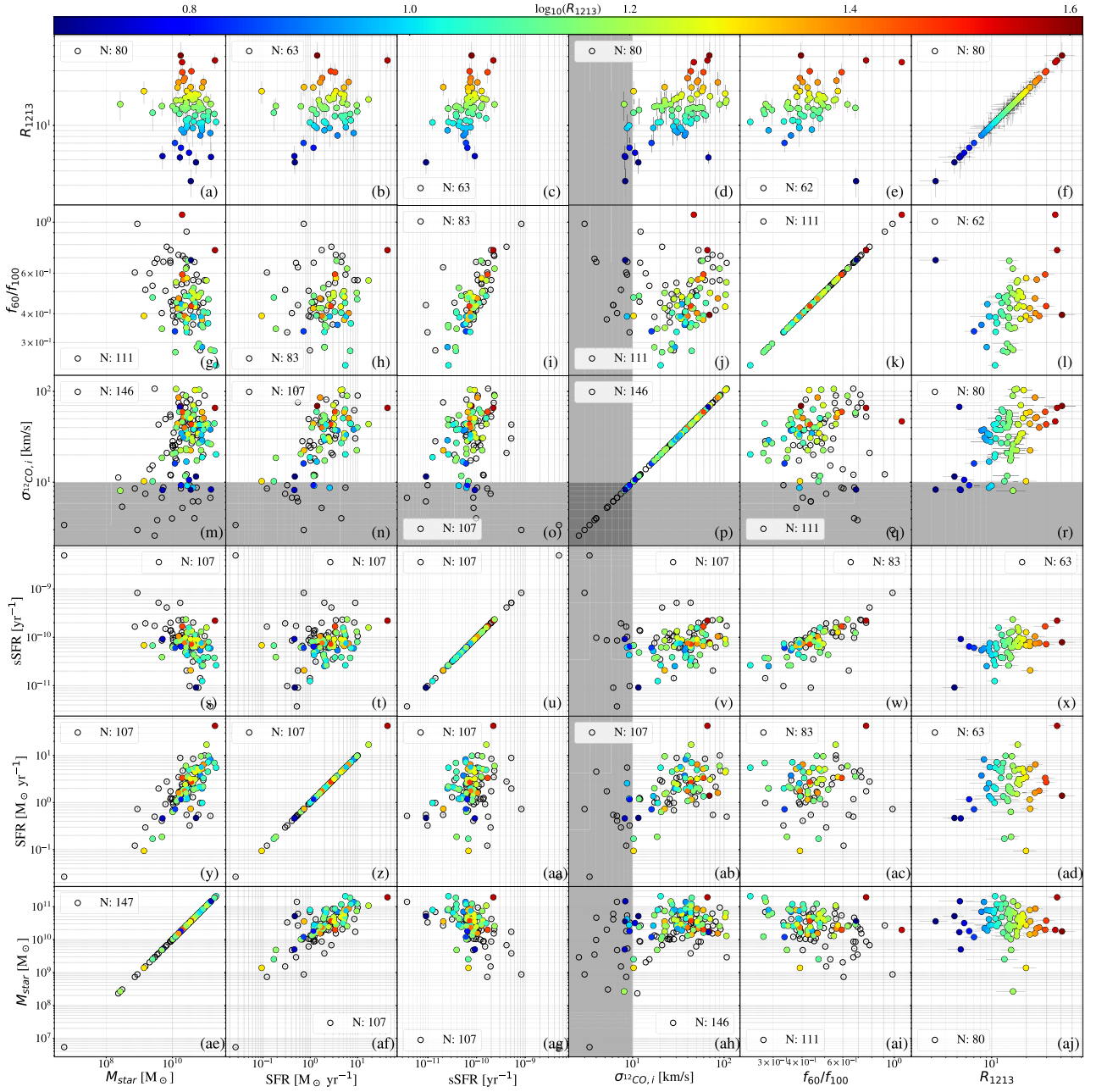
Fig. 3. Correlation plots among six key parameters (from top to bottom and right to left: R_{1213}, f_{60}/f_{100}, $\sigma_{12CO,i}$, sSFR, SFR, and M_{star}). All the galaxies with measurements of both abscissa and ordinate values are indicated as open circles, and filled circles indicate galaxies with R_{1213} and sSFR measurements among them. The colors of the symbols indicate the R_{1213} value. The gray-shaded region indicates $\sigma_{12CO,i} < 10\,\mathrm{km\,s^{-1}}$, the velocity resolution of the COMING data. The number of galaxies with measurements of both abscissa and ordinate values is also indicated in each panel. (Color online)

main sequence (Whitaker et al. 2012) is adopted, where the obtained Pearson's r, Spearman's ρ, and Kendall's τ are 0.41, 0.39, and 0.27, respectively. Since Δ(MS) depends on the definition of the main sequence of SF galaxies, we prefer to use sSFR, a value depending on fewer assumptions, rather than Δ(MS) to see possible variations in physical properties of molecular gas *across* the main sequence of SF galaxies in the following sections.

4 Discussions

We found that R_{1213} somehow relates to sSFR [and Δ(MS)], suggesting that the physical properties of molecular gas traced by ^{12}CO can be different across the main sequence of SF galaxies. Here, we investigate the relationship of R_{1213} with the other physical parameters of galaxies in subsection 4.1, and discuss the causes of the R_{1213} variety in subsections 4.2 and 4.3, and its implications for the variety
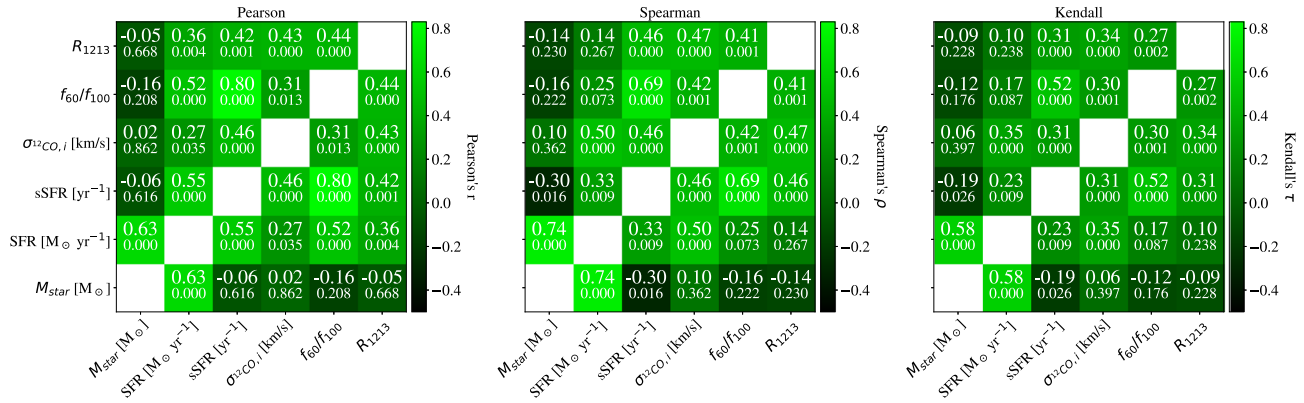
Fig. 4. Correlation coefficients (upper row) and *p*-values (lower row) of the plots in each panel in figure 3 for galaxies with R_{1213} and sSFR measurements. The correlation coefficients are measured by three methods: (a) Pearson's correlation coefficient, *r*; (b) Spearman's rank correlation coefficient, ρ; (c) Kendall's τ coefficient. The pixel color indicates the correlation coefficient value. Note that panel (a) is parametric and panels (b) and (c) are non-parametric methods. Panel (c) is normally more robust than panel (b), and generally (c) < (b) (see the Appendix). (Color online)

in the CO-to-H_2 conversion factor (α_{CO}) in subsection 4.4. We also discuss the possible effects of the α_{CO} variation across the SF main sequence of galaxies on the known relations of sSFR with SFE and μ_{mol} in subsection 4.5.

4.1 Correlation plots for other parameters

In order to investigate the R_{1213}–sSFR relation, we further compare R_{1213} and sSFR with four other parameters including SFR, M_{star}, $\sigma_{12CO,i}$, and f_{60}/f_{100} in figure 3. We focus on these values because SFR and M_{star} are respectively the numerator and denominator of sSFR, and $\sigma_{12CO,i}$ and f_{60}/f_{100} are measures of physical properties of molecular gas such as turbulence and temperature. Figure 4 shows the correlation coefficients of each relation shown in figure 3, which are calculated for galaxies with R_{1213} and sSFR measurements on each panel, i.e., the 63 galaxies indicated as filled circles (or the 62 galaxies for the panels that are related to f_{60}/f_{100}).

We find moderate correlations (correlation coefficients of 0.3–0.5) between R_{1213} and two parameters: $\sigma_{12CO,i}$ and f_{60}/f_{100} (figures 3 and 4). Thus, the R_{1213} variation across the main sequence of SF galaxies is likely to be related to the variations in physical properties of molecular gas. Note that the correlation coefficients do not significantly change even if we simply use σ_{12CO} instead of $\sigma_{12CO,i}$. On the other hand, no correlation is found for the R_{1213}–M_{star} and the R_{1213}–SFR relations. This suggests that the correlation between R_{1213} and sSFR is a consequence of neither a positive correlation between R_{1213} and SFR nor a negative correlation between R_{1213} and M_{star}.

The strongest correlation is found in the f_{60}/f_{100}–sSFR relation. Considering that f_{60}/f_{100} is a measure of dust temperature, this is consistent with previous studies showing higher dust temperature for galaxies with higher sSFR (e.g., Magnelli et al. 2014; Matsuki et al. 2017).

The stronger correlation of the f_{60}/f_{100}–sSFR relation than the R_{1213}–sSFR relation suggests that the former is more fundamental than the latter. Thus, we consider that R_{1213} correlates with sSFR primarily through the correlations of the sSFR–f_{60}/f_{100} and R_{1213}–f_{60}/f_{100} relations.

$\sigma_{12CO,i}$ may also play a role in generating the R_{1213}–sSFR relation. As already mentioned, R_{1213} positively correlates with $\sigma_{12CO,i}$. In panels (o) or (v) of figure 3 (a comparison of $\sigma_{12CO,i}$ and sSFR), we can see that the bulk of galaxies, including those with R_{1213} measurements, are located in the upper left or lower right regions, showing a moderate positive correlation with a Spearman's ρ of 0.46. There also exist some outliers with $\sigma_{12CO,i} \lesssim 10 \, \mathrm{km \, s^{-1}}$ showing a wide range of sSFR. Consequently, the overall correlation becomes quite weak when including those outliers. Note that these trends are still seen even when we use the stacked spectra of only the disk region of galaxies. It should also be noted that the $\sigma_{12CO,i}$ values of the galaxies with $\sigma_{12CO,i} \lesssim 10 \, \mathrm{km \, s^{-1}}$ are upper limits, considering the velocity resolution of $10 \, \mathrm{km \, s^{-1}}$ of the COMING data.

In summary, figures 3 and 4 show that (1) R_{1213} correlates with $\sigma_{12CO,i}$ and f_{60}/f_{100}; (2) the correlation coefficients for the $\sigma_{12CO,i}$–sSFR (0.46) and f_{60}/f_{100}–sSFR (0.69) relations are comparable to or higher than for the R_{1213}–sSFR relation (0.46); and (3) the correlation coefficient for the f_{60}/f_{100}–sSFR relation is higher than that for the $\sigma_{12CO,i}$-sSFR relation. Therefore, the observed trend of R_{1213} along sSFR is considered to be mainly caused by f_{60}/f_{100} with a secondary role for $\sigma_{12CO,i}$, while accurate measurements of $\sigma_{12CO,i}$ and R_{1213} for galaxies with $\sigma_{12CO,i} \lesssim 10 \, \mathrm{km \, s^{-1}}$ are required for a definite conclusion.

4.2 Causes of the R_{1213} variety

As a cause of the R_{1213} variation, four main candidates have been considered since the early studies of R_{1213} in

nearby galaxies: changes in (1) the physical conditions of molecular gas (density, temperature, and opacity); (2) the $[^{12}CO]/[^{13}CO]$ abundance due to selective photodissociation; (3) the $[^{12}CO]/[^{13}CO]$ abundance due to chemical fractionation; and (4) the $^{12}C/^{13}C$ isotope abundance ratio due to stellar nucleosynthesis. We consider that scenario (1) is plausible for the observed R_{1213} variation, at least for our sample galaxies, and scenario (4) may play a secondary role. In this subsection we explain each scenario and the reasons why scenarios (2)–(4) are not expected to play a major role.

R_{1213} can be approximated as a function of the opacity of ^{12}CO (τ_{12CO}) and the abundance ratio of $[^{12}CO]/[^{13}CO]$ under the local thermodynamic equilibrium (LTE) assumption as:[4]

$$R_{1213} \propto \frac{1 - \exp(-\tau_{12CO})}{1 - \exp(-\tau_{13CO})} \sim \frac{1 - \exp(-\tau_{12CO})}{1 - \exp\left(-\frac{\tau_{12CO}}{[^{12}CO]/[^{13}CO]}\right)}, \quad (5)$$

where τ_{13CO} is the optical depth of ^{13}CO. If $h\nu \ll k_B T_k$ (where k_B, ν, and T_k are the Boltzmann constant, line frequency, and kinetic temperature), τ_{12CO} scales as $\propto \frac{N_{12CO}}{\Delta v T_k^2}$, where N_{12CO} and Δv are the ^{12}CO column density and velocity dispersion, respectively. Note that non-LTE analysis also predicts that R_{1213} is a strong function of τ_{12CO} (Cormier et al. 2018). Thus, the R_{1213} variation can be considered to reflect τ_{12CO} variation as a first approximation, and τ_{12CO} is affected by the temperature and turbulence of molecular gas.

Early studies have already noticed a correlation between R_{1213} and f_{60}/f_{100} (e.g., Young & Sanders 1986; Aalto et al. 1995; Crocker et al. 2012; Herrero-Illana et al. 2019; but see also Vila-Vilaro et al. 2015; Cao et al. 2017). They suggested that high gas temperatures and turbulence (as traced by dust temperature) work against large optical depths in ^{12}CO. However, no clear observational evidence has been found for a positive correlation between R_{1213} and the velocity dispersion of the ^{12}CO line. Although there are relevant studies to the R_{1213}–$\sigma_{12CO,i}$ relation, such as the relationships of R_{1213} with the velocity dispersion of the ^{13}CO line (Meier & Turner 2004) and with the inclinations of galaxies (Sage & Isbell 1991), both studies reported null results. In this study we re-examined and confirmed the correlation between R_{1213} and f_{60}/f_{100} with the COMING data, and additionally found a correlation between R_{1213} and $\sigma_{12CO,i}$ when we limited the sample used to investigate the R_{1213}–sSFR correlation. These correlations also support scenario (1), when we assume $\Delta v \sim \sigma_{12CO,i}$.

The abundance ratio of $[^{12}CO]/[^{13}CO]$ can also affect R_{1213}. Scenarios (2)–(4) are processes that change

the $[^{12}CO]/[^{13}CO]$ ratio. Selective photodissociation is expected to be dominant in low-density ($n < 10^2 \, cm^{-3}$) domains or in dense regions with very strong radiation fields (Röllig & Ossenkopf 2013). UV radiation dissociates CO molecules, and ^{13}CO is less effective at self-shielding against UV photons than ^{12}CO due to its lower abundance. Chemical fractionation is expected to become important in deeper regions of molecular clouds where the dust shielding is effective for both ^{12}CO and ^{13}CO. In this region, with a lower temperature of $<35\,K$, ^{13}CO is preferentially formed via the isotopic charge exchange reaction
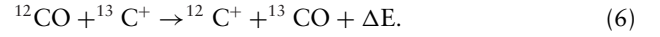
$$^{12}CO + ^{13}C^+ \rightarrow ^{12}C^+ + ^{13}CO + \Delta E. \quad (6)$$

Assuming $[^{12}CO]/[^{13}CO] \sim {}^{12}C/^{13}C$, the $^{12}C/^{13}C$ ratio is also potentially an important factor controlling R_{1213}. The $^{12}C/^{13}C$ ratio is a measure of the ratio of primary to secondary nucleosynthetic components, thus the ratio is expected to decrease as stellar populations evolve, and to depend on the star-formation history (e.g., Audouze et al. 1975), the IMF slope (e.g., Romano et al. 2017), and the treatment of stellar rotation which affects mixing in stars (e.g., Limongi & Chieffi 2018; Romano et al. 2019). It is expected that, in the early evolutionary phase of stellar population, $^{12}C/^{13}C$ is high due to efficient supply of ^{12}C from core-collapse supernovae (SNe) of massive stars, and decreases due to ^{13}C production from intermediate-mass asymptotic giant branch (AGB) stars, then increases due to ^{12}C production from low-mass AGB stars, and decreases again due to type-Ia SNe (e.g., Kobayashi et al. 2011).

There are theoretical and observational studies of R_{1213} in normal galaxies which contradict with scenarios (2)–(4) as a dominant factor changing R_{1213}. Szűcs, Glover, and Klessen (2014) self-consistently calculated R_{1213} for isolated molecular clouds with hydrodynamical simulations taking into account the chemical network, various interstellar radiation fields, and cooling and heating processes. They concluded that selective photodissociation has a minimal effect on R_{1213}, and chemical fractionation can cause a factor of 2–3 decrease. Other theoretical studies also predicted that the photodissociation of the CO molecule is not selective since self-shielding is found not to be important compared to dust and H_2 shielding (Krumholz 2014; Safranek-Shrader et al. 2017).

The observed anticorrelations between R_{1213} and $^{13}CO/C^{18}O$ reported in various galaxies also disfavor the selective photodissociation scenario (e.g., Paglione et al. 2001; Tan et al. 2011), because the rarer $C^{18}O$ is expected to reduce more than ^{13}CO if selective photodissociation is working. It is reported that the radial gradient of R_{1213} in the Milky Way is in the opposite sense of the $^{12}C/^{13}C$ abundance gradient (Paglione et al. 2001). Crocker et al. (2012)

---

[4] Some studies approximate as $R_{1213} \propto \frac{1-\exp(-\tau_{12CO})}{1-\exp(-\tau_{13CO})} \sim \frac{1}{\tau_{13CO}}$ by assuming that τ_{12CO} is large enough (Paglione et al. 2001; Hirota et al. 2010; Cao et al. 2017).

compared several line ratios using six molecular lines and various galaxy properties of ^{12}CO-rich ETGs, and found that correlations between R_{1213} and the galaxy properties were similarly seen even when they used the ^{12}CO/HCN ratio (no difference in the carbon isotope) instead. This suggests that chemical fractionation and ^{12}C/^{13}C variation due to stellar nucleosynthesis are not the dominant processes generating the R_{1213} variation in these ETGs.

However, scenario (4) is likely to become important for extreme dusty SF galaxies such as local ultraluminous infrared galaxies, starburst galaxies (Sliwa et al. 2017; Brown & Wilson 2019), and high-z submillimeter galaxies (Danielson et al. 2013; Zhang et al. 2018). In these galaxies, high R_{1213} and extremely low ^{13}CO/C^{18}O ($\sim$1) values have been found. Given that ^{18}O is produced in massive stars ($\gtrsim 8\,M_\odot$), and assuming ^{13}CO/C^{18}O $\approx$ ^{13}C/^{18}O, ^{13}CO/C^{18}O is expected to be low for young systems or for top-heavy IMF. Indeed, chemical evolution models of galaxies show that such extreme line ratios can be explained by top-heavy IMF (Romano et al. 2017, 2019; Zhang et al. 2018). The observed correlation between R_{1213} and sSFR in this study may suggest that stellar nucleosynthesis is also important, since sSFR can be a measure of the ratio of massive/young and less massive/old stellar populations. The dominant process determining R_{1213} may be different across the SF main sequence. In order to investigate the effect of ^{12}C/^{13}C on the R_{1213} trend across the main sequence, further deep observations in optically thin lines are required.

4.3 Dependence of the six parameters on galaxy morphologies

The turbulent and warm properties of the interstellar medium (ISM) are a natural consequence of galaxies with high sSFR if star-formation feedback plays a major role in determining the ISM properties. Theoretical studies have shown that the molecular clouds are expanded due to feedback by H II regions and are destroyed or displaced by SNe explosion (e.g., Baba et al. 2017; Grisdale et al. 2018). It has also been shown that the observed scaling relations of molecular clouds are reproduced when this feedback is taken into account (e.g., Grisdale et al. 2018; Fujimoto et al. 2019). However, both the spatial and velocity resolutions of our data are not high enough to resolve a single molecular cloud or to discriminate the effects of star-formation feedback from the other larger-scale processes.

The shorter dynamical (or free-fall) timescale than the star-formation timescale (1%–3%, Kennicutt 1998; Leroy et al. 2008) suggests that secular processes are important for star formation in galaxies. It is widely known that bar structures are expected to drive gas inflow by removing angular momentum from the gas, and consequently induce

active star formation at the central regions of galaxies (e.g., Wada & Habe 1995; Sakamoto et al. 1999; Kuno et al. 2007). Galaxy mergers are also a key process, inducing gas condensation and triggering star formation in galaxies (e.g., Sanders & Mirabel 1996; Hopkins et al. 2005). While the enhancement of star formation due to mergers or stellar bars may not be so significant (10%–15%, Rodighiero et al. 2011; Saintonge et al. 2012), both processes help to enhance turbulence and broaden the linewidth of CO emission in galaxies (Sorai et al. 2012; Maeda et al. 2018; Sun et al. 2018; Yajima et al. 2019).

Figure 5 shows histograms of the six key values that are compared in figure 3 for subsamples with different types of bar structures (SA/SAB/SB, de Vaucouleurs et al. 1991), and table 1 summarizes the medians and quartiles of these values for each subsample. The galaxies categorized as "pec" by de Vaucouleurs et al. (1991) are also separately presented in the same figure and table. According to the Kolmogorov–Smirnov (KS) test, there are no significant differences in M_{star} (p-value of 0.9), sSFR (0.07), $\sigma_{^{12}CO,i}$ (0.3), and f_{60}/f_{100} (0.3) between barred (SAB + SB) and non-barred (SA) galaxies, whereas SFR and R_{1213} tend to be higher for barred galaxies than non-barred galaxies, whose p-values are 4×10^{-3} and 3×10^{-2}, respectively. Although the p-values of the KS test are not small enough, the median values of sSFR, $\sigma_{^{12}CO,i}$, and f_{60}/f_{100} are higher for barred galaxies than non-barred galaxies. Therefore, the tendency for galaxies with higher sSFR to have broader $\sigma_{^{12}CO,i}$ obtained in this study might be *partially* attributed to those barred galaxies.

In terms of the morphological peculiarities indicated with the "pec" suffix, on the other hand, we do not find clear differences in any of the six values (figure 5 and table 1). Although no closely interacting galaxies are included in our sample, the morphological peculiarities are generally indicative of galaxy interaction. This suggests that galaxy interaction is unlikely to be a major cause of the wider $\sigma_{^{12}CO,i}$ for galaxies with higher sSFR, at least in our sample. Therefore, high turbulence and temperature are likely to be primarily due to active star formation, and stellar bars might play some partial role in driving the high turbulence of the molecular gas and active star formation via efficient gas inflow.

4.4 Implications of the variation of the CO-to-H$_2$ conversion factor across the main sequence

We adopted a constant α_{CO} to estimate the molecular gas masses of the COMING galaxies in this study, while the R_{1213} variety suggests different α_{CO} among the COMING galaxies. Cormier et al. (2018) showed that the relationship between R_{1213} and α_{CO} is different from galaxy to
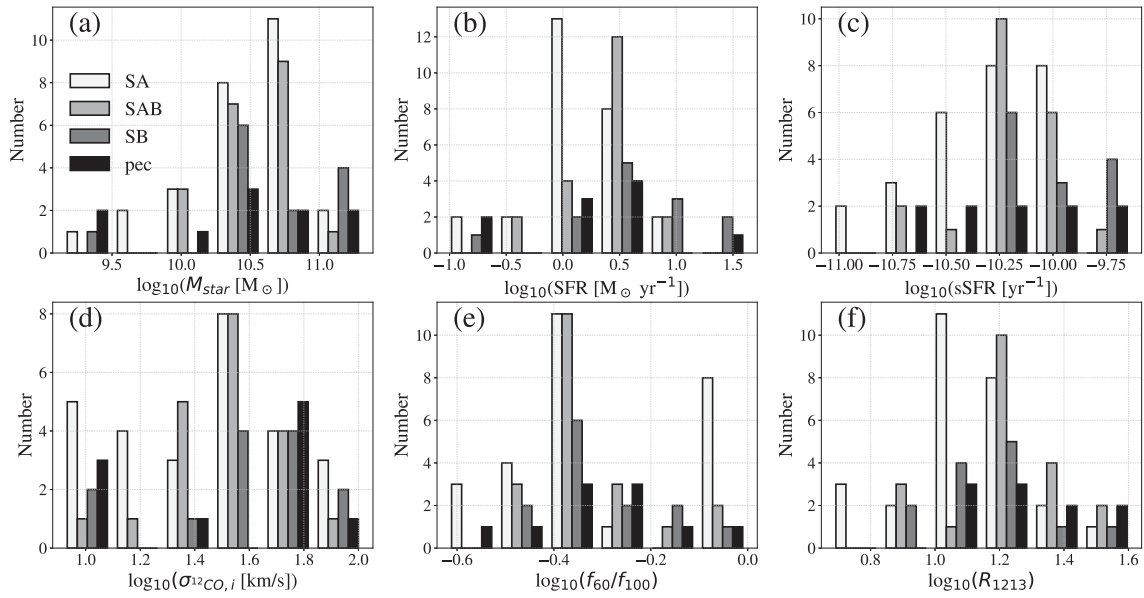
Fig. 5. Histograms of the six key parameters for SA (white), SAB (light gray), and SB (dark gray) galaxies, and those with the "pec" suffix (black).

Table 1. Median and first and third quartiles of the six key parameters in figure 5 for galaxy subsamples with different morphology.

RC3 morphology* Number of galaxies:	SA 27	SAB+SB 33	SAB 20	SB 13	With pec 10	Without pec 53
M_{star} [$10^{10} M_{\odot}$]	3.8[†]	3.8	3.9	3.1	2.8	4.1
	(1.8–7.1)[‡]	(2.4–7.3)	(2.3–6.3)	(2.6–11)	(1.7–6.9)	(2.4–7.3)
SFR [$M_{\odot}$ yr^{-1}]	1.9	3.1	2.7	4.7	2.0	2.4
	(1.2–2.7)	(1.8–5.2)	(1.8–3.8)	(2.0–8.3)	(1.3–3.4)	(1.4–4.9)
sSFR [10^{-11} yr^{-1}]	6.2	7.6	7.3	8.0	6.8	7.3
	(3.8–8.3)	(6.2–9.9)	(6.2–8.9)	(6.7–16)	(4.3–12)	(5.2–8.8)
$\sigma_{12CO,i}$ [km s^{-1}]	31	40	37	44	52	38
	(18–47)	(27–53)	(26–45)	(37–58)	(13–59)	(22–46)
f_{60}/f_{100}	0.41	0.47	0.43	0.48	0.49	0.43
	(0.37–1.00)	(0.40–0.56)	(0.39–0.49)	(0.46–0.57)	(0.41–0.59)	(0.39–0.56)
R_{1213}	12.2	15.3	16.9	14.1	17.1	14.1
	(10.5–14.9)	(13.2–18.6)	(14.2–21.4)	(12.9–16.6)	(13.2–22.8)	(10.8–17.2)

*There are three "S" galaxies among the 63 galaxies, i.e., no classification for bar structures.

[†]Median.

[‡](First quartile–third quartile).

galaxy, while their non-LTE radiative transfer calculations with RADEX (van der Tak et al. 2007) predict a clear anticorrelation between these two values, which is ascribed to τ_{12CO} variation (Sandstrom et al. 2013). Indeed, Accurso et al. (2017) found that α_{CO} depends not only on metallicity but also on Δ(MS). In this subsection we discuss the possible variation in α_{CO} and its impact on our results. Our data show that galaxies with high sSFR tend to have high R_{1213}, suggesting low τ_{12CO} owing to high gas temperature and large linewidths. According to magnetohydrodynamic simulations of molecular clouds, it is claimed that α_{CO} scales with temperature and ^{12}CO linewidth as $\propto T^{-1/2}$

and $\propto \Delta v^{-1/2}$, respectively (Shetty et al. 2011). The dust temperatures of the COMING galaxies inferred from f_{60}/f_{100} and a conventional modified black-body model (opacity of $\kappa_0 = 0.009$ cm^2 g^{-1} at $\nu_0 = 200$ GHz, and emissivity index of $\beta = 1.8$) lie in the range 25–40 K; $\sigma_{12CO,i}$ lies in the range $\sim$10–100 km s^{-1}, although there also exist low-$\sigma_{12CO,i}$ ($<$10 km s^{-1}) galaxies in our sample. Assuming gas temperature equals dust temperature and $\Delta v \sim \sigma_{12CO,i}$, these varieties could impose a variation in α_{CO} by a factor of $\sim$4 *at most* for our sample. Thus, the correlations between R_{1213} and μ_{mol} in figure 1c would actually be weaker than when obtained using a constant α_{CO}. With a sophisticated

technique for deriving α_{CO} using CO, H I, and dust maps of galaxies (Leroy et al. 2011; Sandstrom et al. 2013), α_{CO} variations among the COMING galaxies are investigated in a forthcoming paper (A. Yasuda et al. in preparation).

There are three caveats here: (1) the resolutions of our data are not spatially or spectroscopically high enough to resolve a single molecular cloud; (2) the "luminosity-weighted" dust temperature does not necessarily reflect the temperature of the bulk of the molecular gas; and (3) the contribution from diffuse molecular gas. The kpc-scale beam encompasses multiple molecular clouds, and the observed velocity dispersion is likely to reflect inter-cloud velocity dispersion rather than that of a single cloud. Additionally, the dust temperature derived by SED fitting is "luminosity-weighted" temperature rather than mass-weighted (Scoville et al. 2014, 2016). But, the ranges of velocity dispersion and temperature we assumed here are not significantly different from the observed values for molecular clouds. It is known that the velocity dispersions of molecular clouds including those at the central region of the Milky Way lie in the range 1–100 km s^{-1} (e.g., Oka et al. 2001). Multi-transition CO observations have revealed that the temperature of molecular clouds is reported in the range 10–20 K for quiescent clouds to 15–100 K for clouds with H II regions in M 33 (Wilson et al. 1997). The assumed variations of Δv and T here are not so inadequate to consider the possible maximum variation in the α_{CO} value.

For the third point, several studies of both Milky Way clouds and extragalactic objects have suggested that a non-negligible fraction of ^{12}CO comes from the diffuse molecular component ($\sim$30%; e.g., Wilson & Walker 1994; Rosolowsky et al. 2007; Sawada et al. 2012; Pety et al. 2013; Morokuma-Matsui et al. 2015; Maeda et al. 2020; Liszt 2020). This diffuse molecular component is considered to consist of volume-filling diffuse molecular gas and/or the envelopes of molecular clouds (Wilson & Walker 1994; Meier et al. 2000; Pety et al. 2013). Considering that the diffuse component tends to have a large velocity dispersion (Garcia-Burillo et al. 1992; Pety et al. 2013; Caldú-Primo et al. 2013), the positive correlations of the sSFR–$\sigma_{^{12}CO,i}$ and R_{1213}–$\sigma_{^{12}CO,i}$ relations indicate a larger fraction of the diffuse component for galaxies with high sSFR and R_{1213}. The CO-to-H$_2$ conversion factor is reported to be similar in diffuse and dense molecular gas *on average*, with a large scatter in the Milky Way because the small abundance ratio of [CO]/[H$_2$] in diffuse gas is compensated by a much higher brightness per CO molecule (Liszt et al. 2010; Liszt & Pety 2012). However, it is important to investigate the fraction of the diffuse molecular-gas component of galaxies as a function of sSFR to understand the α_{CO} variation across the main sequence of SF galaxies.

4.5 Implications of galaxy evolution on the SFR–mass parameter space and high-redshift galaxies

Our results suggest that there might be variation in α_{CO} across the SF main sequence as a consequence of the differences in temperature and degree of turbulence of molecular gas in galaxies, at least for the local Universe. This further suggests that one may need to pay special attention when discussing which of μ_{mol} or SFE is the dominant factor controlling sSFR [or Δ(MS)]. Previous studies found that Δ(MS) and sSFR are correlated with both μ_{mol} and SFE, i.e., galaxies with higher SFR at fixed M_{star} have more abundant molecular gas and form stars more efficiently from the molecular gas (Saintonge et al. 2012; Genzel et al. 2015; Scoville et al. 2017; Tacconi et al. 2018). The possible α_{CO} variation by a factor of $\sim$4 is unlikely to completely extinguish the reported correlations between sSFR and μ_{mol} or SFE, since the correlations are found over more than two orders of magnitude of both values. However, a magnitude relationship of the strength of the known positive correlations between sSFR and μ_{mol} or SFE can be affected, since M_{mol} is the numerator and denominator of μ_{mol} and SFE, respectively. If galaxies with higher sSFR tend to have lower α_{CO}, SFE would become relatively more important for the sSFR [or Δ(MS)] variation than μ_{mol}, as claimed by Ellison et al. (2020a).

The redshift evolution of α_{CO} can be discussed in the same context combined with the redshift evolution of metallicity. The sSFR of the main-sequence galaxies at fixed M_{star} is known to increase as redshift increases (e.g., Whitaker et al. 2012; Speagle et al. 2014), making one expect higher ISM turbulence and temperature in higher-redshift galaxies from this study. Indeed, high-redshift galaxies tend to have more highly turbulent molecular gas (Genzel et al. 2013; Übler et al. 2018; Girard et al. 2019), higher dust temperature (Magdis et al. 2012; Magnelli et al. 2014; Schreiber et al. 2018), and lower metallicity (e.g., Savaglio et al. 2005; Shapley et al. 2005; Erb et al. 2006; Liu et al. 2008; Maiolino et al. 2008; Mannucci et al. 2009; Yuan et al. 2013; Steidel et al. 2014) than local galaxies. With a Milky Way type α_{CO}, a much larger μ_{mol} value is reported in galaxies at $z \sim$ 1–2 ($\sim$50%, e.g., Daddi et al. 2010; Tacconi et al. 2013, 2020; Genzel et al. 2013; Riechers et al. 2020, and references therein) than local galaxies ($\lesssim$5%–10%, e.g., Saintonge et al. 2011, 2017; Bolatto et al. 2017; Sorai et al. 2019). Since μ_{mol} is one of the key parameters to constrain both star-formation and feedback models in cosmological simulations and semi-analytic models of galaxy formation (e.g., Popping et al. 2012, 2014, 2015; Morokuma-Matsui & Baba 2015; Saintonge et al. 2017), accurate α_{CO} estimation at higher redshifts is essential.

Taking the three parameters (metallicity, velocity dispersion, and temperature) into consideration, we roughly estimate α_{CO} of galaxies at high redshifts. For galaxies with $M_{star} \sim 10^{10.5} M_\odot$ at $z \sim 1.5$, the metallicity, velocity dispersion of molecular gas, and dust temperature can be respectively ~ 0.2 dex lower (Yabe et al. 2014; Zahid et al. 2014; Kashino et al. 2017),[5] ~ 5 times higher (Genzel et al. 2013), and only ~ 1.2 times higher than local counterparts. In this case, the effects of metallicity and temperature are negligible (Bolatto et al. 2013), and α_{CO} could become lower than the local value by a factor of 2. Indeed, Carleton et al. (2017) obtained comparable α_{CO} for galaxies at $1 < z < 1.5$ to the local galaxies when they assumed several models for the redshift evolution of SFE. Future high-spatial-resolution and hig-velocity-resolution observations in ^{12}CO of high-redshift galaxies would shed light on the α_{CO} variation across the SF main sequence of galaxies as a function of redshift.

5 Summary

Using the ^{12}CO and ^{13}CO mapping data obtained in the COMING project, we have investigated the relationship between R_{1213} and sSFR combined with four other parameters (M_{star}, SFR, f_{60}/f_{100}, and $\sigma_{12CO,i}$) of local star-forming galaxies to understand the molecular gas properties traced with the ^{12}CO line on the SFR–mass relation of galaxies. Owing to the stacking analysis, ^{13}CO emission was successfully detected in 80 galaxies out of the 147 COMING galaxies. The results obtained and their implications are as follows:

- The error-weighted mean of R_{1213} for the 80 COMING galaxies with measurements of ^{12}CO and ^{13}CO is 10.9 with a standard deviation of 7.0, which is consistent with previous studies on R_{1213} of local SF galaxies (section 3, figure 2).
- R_{1213} moderately correlates with sSFR with a Spearman's rank correlation coefficient of 0.46 (section 3, figure 2).
- R_{1213} variation is likely to be attributed to τ_{12CO} variation, which is supported by the positive correlations of the R_{1213}–f_{60}/f_{100} and R_{1213}–$\sigma_{12CO,i}$ relations for galaxies with R_{1213} measurements (subsection 4.1, figures 3 and 4).
- The correlations of the sSFR–f_{60}/f_{100} and sSFR–$\sigma_{12CO,i}$ relations for galaxies with R_{1213} measurements suggest that high turbulence and temperature of ISM are related to active star formation (subsection 4.1, figures 3 and 4). Stellar bars might play some role in enhancing the

turbulence and inducing active star formation in the central regions of galaxies via gas inflow, which is supported by slightly larger median values of $\sigma_{12CO,i}$ and sSFR for barred galaxies than non-barred galaxies in our sample, although there is a large overlap between them (subsection 4.3, figure 5, and table 1).
- The variation in the dust temperature inferred from f_{60}/f_{100} and the observed velocity dispersion of molecular gas in the COMING galaxies can impose α_{CO} variation by a factor of ~ 4 *at most* according to the relation of $\alpha_{CO} \propto T^{-1/2} \Delta v^{-1/2}$ predicted in numerical simulations of molecular clouds (subsections 4.2 and 4.4).
- The inferred α_{CO} variation is not likely to completely extinguish the correlations between sSFR and μ_{mol} or SFE reported in the literature. However, a magnitude relationship of the strength of the positive correlations between sSFR and μ_{mol} or SFE can be affected, since M_{mol} is the numerator and denominator for μ_{mol} and SFE, respectively (subsection 4.5).

Appendix. Possibility of fake correlation for the R_{1213}–sSFR relation

We find a moderate correlation between R_{1213} and sSFR for the 63 galaxies, but no correlation for the R_{1213}–SFR (the numerator of sSFR) and R_{1213}–M_{star} (the denominator of sSFR) relations in this study. In order to examine whether or not the obtained correlation of the R_{1213}–sSFR relation is fake due to the small number of galaxies, we generated 10000 sets of mock galaxy samples based on the mean vector and the variance-covariance matrix obtained from

---

[5] At this redshift, massive systems with $M_{star} \sim 10^{11} M_\odot$ are known to already be enriched to the level observed in local counterparts (Zahid et al. 2014; Kashino et al. 2017).
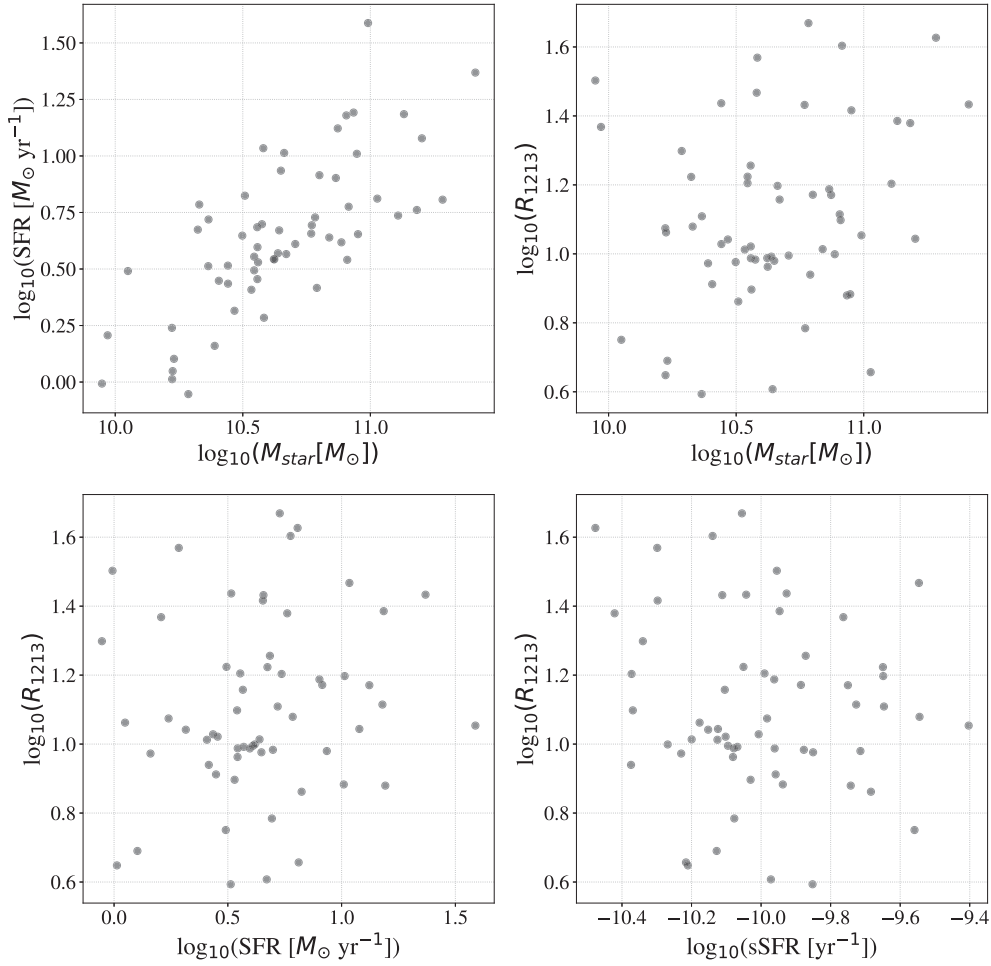
Fig. 6. Example of the three-parameter set of the generated 60 mock galaxies and resultant R_{1213}–sSFR relation. (Color online)
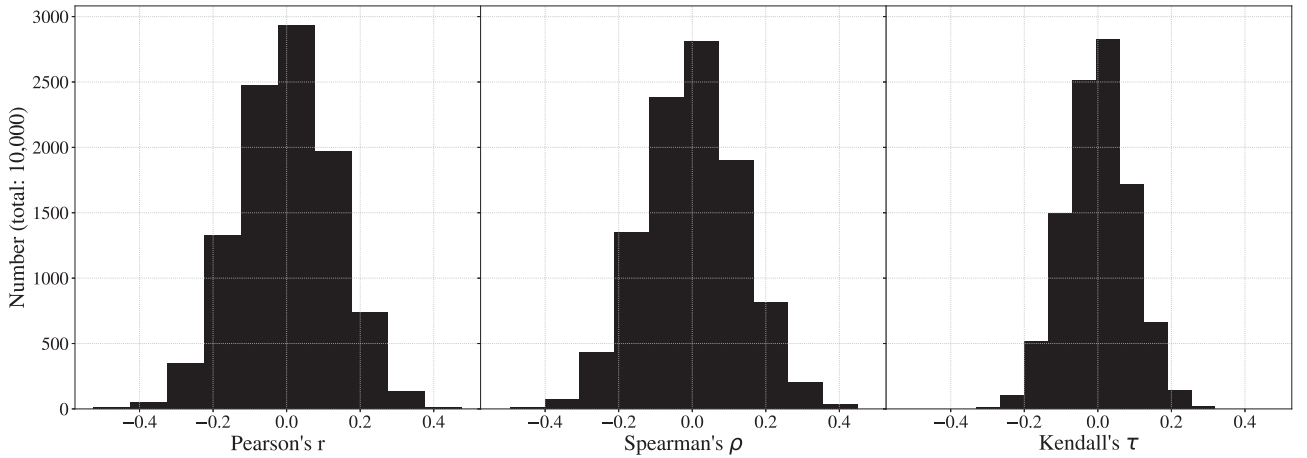

Fig. 7. Histograms of the resultant correlation coefficients for each method when generating mock samples 10000 times.

the observed M_{star}, SFR, and R_{1213} values of the COMING galaxies using the `Multivariate_normal` function of the Python module `Numpy`. For the number of galaxies in each set, three cases are considered: 60, 100, and 1000. Then we manually set the covariances of the R_{1213}–M_{star} and

R_{1213}–SFR relations to be zero. The relationship among these three values of a mock galaxy sample is shown in figure 6. Using these 10000 mock data sets, we calculated the sSFR and the correlation coefficients of the resultant R_{1213}–sSFR relation.

Figure 7 shows a histogram of the values obtained for Pearson's r, Spearman's ρ, and Kendall's τ for the 10000 mock data sets. The largest r, ρ, and τ are 0.48, 0.45, and 0.32, respectively. The numbers of mock datasets with larger correlation coefficients than the observed values are 5 for Pearson's r, 0 for Spearman's ρ, and 3 for Kendall's τ, i.e., p-values of 3×10^{-4}, 0×10^{-4}, and 1×10^{-4}. We also find that the histograms become sharper for the larger number of galaxies in each dataset. This result shows that the probability of fake correlation reduces as the number of galaxy samples increases. The sample number of 63 in this study is large enough to conclude that the obtained positive correlation between R_{1213} and sSFR with correlation coefficients ~ 0.4 is not fake.

References

Aalto, S., Beswick, R., & Jütte, E. 2010, A&A, 522, A59

Aalto, S., Black, J. H., Johansson, L. E. B., & Booth, R. S. 1991, A&A, 249, 323

Aalto, S., Booth, R. S., Black, J. H., & Johansson, L. E. B. 1995, A&A, 300, 369

Aalto, S., Booth, R. S., Black, J. H., Koribalski, B., & Wielebinski, R. 1994, A&A, 286, 365

Aalto, S., Radford, S. J. E., Scoville, N. Z., & Sargent, A. I. 1997, ApJ, 475, L107

Accurso, G., et al. 2017, MNRAS, 470, 4750

Alatalo, K., et al. 2015, MNRAS, 450, 3874

Audouze, J., Lequeux, J., & Vigroux, L. 1975, A&A, 43, 71

Baba, J., Morokuma-Matsui, K., & Saitoh, T. R. 2017, MNRAS, 464, 246

Becker, R., & Freudling, W. 1991, A&A, 251, 454

Béthermin, M., et al. 2018, A&A, 620, A115

Blitz, L., Magnani, L., & Mundy, L. 1984, ApJ, 282, L9

Bolatto, A. D., et al. 2017, ApJ, 846, 159

Bolatto, A. D., Wolfire, M., & Leroy, A. K. 2013, ARA&A, 51, 207

Braine, J., Combes, F., & van Driel, W. 1993, A&A, 280, 451

Brown, T., & Wilson, C. D. 2019, ApJ, 879, 17

Caldú-Primo, A., Schruba, A., Walter, F., Leroy, A., Sandstrom, K., de Blok, W. J. G., Ianjamasimanana, R., & Mogotsi, K. M. 2013, AJ, 146, 150

Cao, Y., Wong, T., Xue, R., Bolatto, A. D., Blitz, L., Vogel, S. N., Leroy, A. K., & Rosolowsky, E. 2017, ApJ, 847, 33

Carleton, T., et al. 2017, MNRAS, 467, 4886

Casasola, V., et al. 2017, A&A, 605, A18

Casoli, F., Dupraz, C., & Combes, F. 1992, A&A, 264, 55

Cormier, D., et al. 2018, MNRAS, 475, 3909

Crocker, A., et al. 2012, MNRAS, 421, 1298

Daddi, E., et al. 2007, ApJ, 670, 156

Daddi, E., et al. 2010, ApJ, 713, 686

Danielson, A. L. R., et al. 2013, MNRAS, 436, 2793

Davis, T. A. 2014, MNRAS, 445, 2378

de Vaucouleurs, G., de Vaucouleurs, A., Corwin, H. G., Jr., Buta, R. J., Paturel, G., & Fouque, P. 1991, Third Reference Catalogue of Bright Galaxies, Vol. I–III (New York: Springer)

Dickman, R. L. 1978, ApJS, 37, 407

Eckart, A., Cameron, M., Rothermel, H., Wild, W., Zinnecker, H., Rydbeck, G., Olberg, M., & Wiklind, T. 1990, ApJ, 363, 451

Elbaz, D., et al. 2007, A&A, 468, 33

Ellison, S. L., et al. 2020a, MNRAS, 493, L39

Ellison, S. L., Thorp, M. D., Pan, H.-A., Lin, L., Scudder, J. M., Bluck, A. F. L., Sánchez, S. F., & Sargent, M. 2020b, MNRAS, 492, 6027

Encrenaz, P. J., Stark, A. A., Combes, F., & Wilson, R. W. 1979, A&A, 78, L1

Erb, D. K., Shapley, A. E., Pettini, M., Steidel, C. C., Reddy, N. A., & Adelberger, K. L. 2006, ApJ, 644, 813

Frerking, M. A., Langer, W. D., & Wilson, R. W. 1982, ApJ, 262, 590

Fujimoto, Y., Chevance, M., Haydon, D. T., Krumholz, M. R., & Kruijssen, J. M. D. 2019, MNRAS, 487, 1717

Garay, G., Mardones, D., & Mirabel, I. F. 1993, A&A, 277, 405

Garcia-Burillo, S., Guelin, M., Cernicharo, J., & Dahlem, M. 1992, A&A, 266, 21

Genzel, R., et al. 2013, ApJ, 773, 68

Genzel, R., et al. 2015, ApJ, 800, 20

Girard, M., Dessauges-Zavadsky, M., Combes, F., Chisholm, J., Patrício, V., Richard, J., & Schaerer, D. 2019, A&A, 631, A91

Gordon, M. A., & Burton, W. B. 1976, ApJ, 208, 346

Grisdale, K., Agertz, O., Renaud, F., & Romeo, A. B. 2018, MNRAS, 479, 3167

Halfen, D. T., Woolf, N. J., & Ziurys, L. M. 2017, ApJ, 845, 158

Henkel, C., Downes, D., Weiß, A., Riechers, D., & Walter, F. 2010, A&A, 516, A111

Herrero-Illana, R., et al. 2019, A&A, 628, A71

Hirota, A., Kuno, N., Sato, N., Nakanishi, H., Tosaki, T., & Sorai, K. 2010, PASJ, 62, 1261

Hopkins, P. F., Hernquist, L., Cox, T. J., Di Matteo, T., Martini, P., Robertson, B., & Springel, V. 2005, ApJ, 630, 705

Kashino, D., et al. 2017, ApJ, 835, 88

Kennicutt, R. C., Jr. 1998, ApJ, 498, 541

Kikumoto, T., Taniguchi, Y., Nakai, N., Ishizuki, S., Matsushita, S., & Kawabe, R. 1998, PASJ, 50, 309

Knapp, G. R., & Bowers, P. F. 1988, ApJ, 331, 974

Kobayashi, C., Karakas, A. I., & Umeda, H. 2011, MNRAS, 414, 3231

Koyama, S., et al. 2017, ApJ, 847, 137

Koyama, S., et al. 2019, ApJ, 874, 142

Kroupa, P. 2001, MNRAS, 322, 231

Kroupa, P., & Weidner, C. 2003, ApJ, 598, 1076

Krumholz, M. R. 2014, MNRAS, 437, 1662

Kuno, N., et al. 2007, PASJ, 59, 117

Lada, C. J., Lada, E. A., Clemens, D. P., & Bally, J. 1994, ApJ, 429, 694

Lee, B., & Chung, A. 2018, ApJ, 866, L10

Leitherer, C., et al. 1999, ApJS, 123, 3

Leroy, A. K., et al. 2011, ApJ, 737, 12

Leroy, A. K., Walter, F., Brinks, E., Bigiel, F., de Blok, W. J. G., Madore, B., & Thornley, M. D. 2008, AJ, 136, 2782

Limongi, M., & Chieffi, A. 2018, ApJS, 237, 13

Lin, L., et al. 2017, ApJ, 851, 18

Liszt, H. S. 2020, ApJ, 897, 104

Liszt, H. S., & Pety, J. 2012, A&A, 541, A58

Liszt, H. S., Pety, J., & Lucas, R. 2010, A&A, 518, A45

Liu, X., Shapley, A. E., Coil, A. L., Brinchmann, J., & Ma, C.-P. 2008, ApJ, 678, 758

Maeda, F., Ohta, K., Fujimoto, Y., Habe, A., & Baba, J. 2018, PASJ, 70, 37

Maeda, F., Ohta, K., Fujimoto, Y., Habe, A., & Ushio, K. 2020, MNRAS, 495, 3840

Magdis, G. E., et al. 2012, ApJ, 760, 6

Magnelli, B., et al. 2014, A&A, 561, A86

Maiolino, R., et al. 2008, A&A, 488, 463

Mannucci, F., et al. 2009, MNRAS, 398, 1915

Martin, D. C., et al. 2005, ApJ, 619, L1

Matsuki, Y., Koyama, Y., Nakagawa, T., & Takita, S. 2017, MNRAS, 466, 2517

Matsushita, S., Kohno, K., Vila-Vilaro, B., Tosaki, T., & Kawabe, R. 1998, ApJ, 495, 267

Meier, D. S., & Turner, J. L. 2004, AJ, 127, 2069

Meier, D. S., Turner, J. L., & Hurt, R. L. 2000, ApJ, 531, 200

Milam, S. N., Savage, C., Brewster, M. A., Ziurys, L. M., & Wyckoff, S. 2005, ApJ, 634, 1126

Morokuma-Matsui, K., & Baba, J. 2015, MNRAS, 454, 3792

Morokuma-Matsui, K., Sorai, K., Watanabe, Y., & Kuno, N. 2015, PASJ, 67, 2

Noeske, K. G., et al. 2007, ApJ, 660, L43

Oka, T., Hasegawa, T., Sato, F., Tsuboi, M., Miyazaki, A., & Sugimoto, M. 2001, ApJ, 562, 348

Paglione, T. A. D., et al. 2001, ApJS, 135, 183

Papadopoulos, P. P., & Seaquist, E. R. 1998, ApJ, 492, 521

Papadopoulos, P. P., & Seaquist, E. R. 1999, ApJ, 516, 114

Pety, J., et al. 2013, ApJ, 779, 43

Polk, K. S., Knapp, G. R., Stark, A. A., & Wilson, R. W. 1988, ApJ, 332, 432

Popping, G., Behroozi, P. S., & Peeples, M. S. 2015, MNRAS, 449, 477

Popping, G., Caputi, K. I., Somerville, R. S., & Trager, S. C. 2012, MNRAS, 425, 2386

Popping, G., Somerville, R. S., & Trager, S. C. 2014, MNRAS, 442, 2398

Rickard, L. J., Palmer, P., Morris, M., Turner, B. E., & Zuckerman, B. 1977, ApJ, 213, 673

Rickard, L. J., Palmer, P., Morris, M., Zuckerman, B., & Turner, B. E. 1975, ApJ, 199, L75

Riechers, D. A., et al. 2020, ApJ, 896, L21

Rodighiero, G., et al. 2011, ApJ, 739, L40

Röllig, M., & Ossenkopf, V. 2013, A&A, 550, A56

Romano, D., Matteucci, F., Zhang, Z.-Y., Ivison, R. J., & Ventura, P. 2019, MNRAS, 490, 2838

Romano, D., Matteucci, F., Zhang, Z. Y., Papadopoulos, P. P., & Ivison, R. J. 2017, MNRAS, 470, 401

Rosolowsky, E., Keto, E., Matsushita, S., & Willner, S. P. 2007, ApJ, 661, 830

Safranek-Shrader, C., Krumholz, M. R., Kim, C.-G., Ostriker, E. C., Klein, R. I., Li, S., McKee, C. F., & Stone, J. M. 2017, MNRAS, 465, 885

Sage, L. J. 1990, A&A, 239, 125

Sage, L. J., & Isbell, D. W. 1991, A&A, 247, 320

Saintonge, A., et al. 2011, MNRAS, 415, 32

Saintonge, A., et al. 2012, ApJ, 758, 73

Saintonge, A., et al. 2017, ApJS, 233, 22

Sakamoto, K., Okumura, S. K., Ishizuki, S., & Scoville, N. Z. 1999, ApJ, 525, 691

Sakamoto, S., Handa, T., Sofue, Y., Honma, M., & Sorai, K. 1997, ApJ, 475, 134

Sakamoto, S., Hayashi, M., Hasegawa, T., Handa, T., & Oka, T. 1994, ApJ, 425, 641

Salpeter, E. E. 1955, ApJ, 121, 161

Sanders, D. B., Mazzarella, J. M., Kim, D. C., Surace, J. A., & Soifer, B. T. 2003, AJ, 126, 1607

Sanders, D. B., & Mirabel, I. F. 1996, ARA&A, 34, 749

Sandqvist, A., Elfhag, T., & Jorsater, S. 1988, A&A, 201, 223

Sandstrom, K. M., et al. 2013, ApJ, 777, 5

Savaglio, S., et al. 2005, ApJ, 635, 260

Sawada, T., Hasegawa, T., Sugimoto, M., Koda, J., & Handa, T. 2012, ApJ, 752, 118

Schreiber, C., et al. 2018, A&A, 609, A30

Schruba, A., et al. 2011, AJ, 142, 37

Scoville, N., et al. 2014, ApJ, 783, 84

Scoville, N., et al. 2016, ApJ, 820, 83

Scoville, N., et al. 2017, ApJ, 837, 150

Shapley, A. E., Coil, A. L., Ma, C.-P., & Bundy, K. 2005, ApJ, 635, 1006

Sheth, K., et al. 2010, PASP, 122, 1397

Shetty, R., Glover, S. C., Dullemond, C. P., Ostriker, E. C., Harris, A. I., & Klessen, R. S. 2011, MNRAS, 415, 3253

Sliwa, K., Wilson, C. D., Aalto, S., & Privon, G. C. 2017, ApJ, 840, L11

Solomon, P. M., & de Zafra, R. 1975, ApJ, 199, L79

Solomon, P. M., Scoville, N. Z., & Sanders, D. B. 1979, ApJ, 232, L89

Sorai, K., et al. 2012, PASJ, 64, 51

Sorai, K., et al. 2019, PASJ, 71, S14

Speagle, J. S., Steinhardt, C. L., Capak, P. L., & Silverman, J. D. 2014, ApJS, 214, 15

Spilker, J. S., et al. 2014, ApJ, 785, 149

Stark, A. A., & Carlson, E. R. 1984, ApJ, 279, 122

Steidel, C. C., et al. 2014, ApJ, 795, 165

Sun, J., et al. 2018, ApJ, 860, 172

Szűcs, L., Glover, S. C. O., & Klessen, R. S. 2014, MNRAS, 445, 4055

Tacconi, L. J., et al. 2013, ApJ, 768, 74

Tacconi, L. J., et al. 2018, ApJ, 853, 179

Tacconi, L. J., Genzel, R., & Sternberg, A. 2020, arXiv:2003.06245

Tan, Q.-H., Gao, Y., Zhang, Z.-Y., & Xia, X.-Y. 2011, Res. Astron. Astrophys., 11, 787

Taniguchi, Y., & Ohyama, Y. 1998, ApJ, 507, L121

Übler, H., et al. 2018, ApJ, 854, L24

van der Tak, F. F. S., Black, J. H., Schöier, F. L., Jansen, D. J., & van Dishoeck, E. F. 2007, A&A, 468, 627

Vila-Vilaro, B., Cepa, J., & Zabludoff, A. 2015, ApJS, 218, 28

Wada, K., & Habe, A. 1995, MNRAS, 277, 433

Watanabe, Y., Sorai, K., Kuno, N., & Habe, A. 2011, MNRAS, 411, 1409

Weliachew, L., Casoli, F., & Combes, F. 1988, A&A, 199, 29

Wen, X.-Q., Wu, H., Zhu, Y.-N., Lam, M. I., Wu, C.-J., Wicker, J., & Zhao, Y.-H. 2013, MNRAS, 433, 2946

Whitaker, K. E., van Dokkum, P. G., Brammer, G., & Franx, M. 2012, ApJL, 754, L29

Wild, W., Eckart, A., & Wiklind, T. 1997, A&A, 322, 419

Wilson, C. D., & Walker, C. E. 1994, ApJ, 432, 148

Wilson, C. D., Walker, C. E., & Thornley, M. D. 1997, ApJ, 483, 210

Wright, E. L., et al. 2010, AJ, 140, 1868

Wright, M. C. H., Ishizuki, S., Turner, J. L., Ho, P. T. P., & Lo, K. Y. 1993, ApJ, 406, 470

Wuyts, S., et al. 2011, ApJ, 738, 106

Xie, S., Young, J., & Schloerb, F. P. 1994, ApJ, 421, 434

Yabe, K., et al. 2014, MNRAS, 437, 3647

Yajima, Y., et al. 2019, PASJ, 71, S13

Young, J. S., & Sanders, D. B. 1986, ApJ, 302, 680

Young, J. S., & Scoville, N. 1982, ApJ, 258, 467

Young, J. S., & Scoville, N. Z. 1984, ApJ, 287, 153

Yuan, T. T., Kewley, L. J., & Richard, J. 2013, ApJ, 763, 9

Zahid, H. J., et al. 2014, ApJ, 792, 75

Zhang, Z.-Y., Romano, D., Ivison, R. J., Papadopoulos, P. P., & Matteucci, F. 2018, Nature, 558, 260